

Propagation and Radiation Characteristics of Multilayer Coupled-Line Bandpass Filters Using Conductor-Backed Coplanar Transmission Lines

Chi-Jung Kuo¹, Chong-Yi Liou², and Shau-Gang Mao², *

Abstract—This paper presents the analytical design formulas for the bandpass filters which are built on the asymmetrically coupled-line conductor-backed coplanar transmission lines (CBCTLs) in multilayer configuration. The full-wave simulation is employed to characterize the far-field patterns of space-wave and surface-wave radiations as well as the frequency-dependent conductor, dielectric, and radiation losses. Good agreement among the results of full-wave simulation, transmission-line model, and measurement justifies the design procedure and validates the analytical design formulas. By properly placing the dielectric materials in multilayer configuration, a bandpass filter for minimizing the radiated power loss and improving the stopband characteristic can be achieved.

1. INTRODUCTION

High-performance filters represent a critical and substantive portion of any communication system [1–7]. To improve the filter performance in the microwave and millimeter-wave regimes, the power losses due to conduction and radiation must be reduced as low as possible [8–11]. The requisite weak coupling in the conventional end-coupled microstrip or CPW filters for narrower bandwidth are usually realized by keeping the resonant elements far apart, which results in the undesirable radiation effect from gap discontinuities and leads to the primary cause of losses in the millimeter-wave range [12–15]. Although the unwanted radiation can be suppressed by adopting housing, this would inevitably increase the engineering cost and deteriorate the upper stopband of a filter due to the excitation of waveguide modes [16, 17].

Recently, there has been increasing interest in multilayer bandpass filters to meet the challenges of size, performance, and cost requirements [18–25]. However, most of the multilayer filters were analyzed by quasi-static or full-wave methods [10, 18], and their designs have been limited to the quarter-wavelength coupled-line sections only [22]. Furthermore, the multilayer bandpass filters utilizing aperture coupling on common ground seem to require an elaborate package [24]. These studies did not consider the loss mechanism, such as the losses due to dielectric, conductor, and radiation in multilayer configuration.

In this paper, the filter structures implemented by the overlapped-gap-coupled coplanar transmission lines on the multilayer dielectric substrate with back conductor are investigated theoretically and experimentally. Specifically, the far-field radiating gain patterns and the power loss mechanisms caused by conductor, dielectric, and radiation are further investigated. Moreover, the design formulas for the multilayer bandpass filters are presented. The utilization of the backside metallization in the CBCTLs [26] not only enhances mechanical strength and facilitates heat sink, but

Received 27 February 2015, Accepted 22 April 2015, Scheduled 19 June 2015

* Corresponding author: Shau-Gang Mao (sgmao@ntu.edu.tw).

¹ Graduate Institute of Computer and Communication Engineering, National Taipei University of Technology, Taipei 106, Taiwan.

² Department of Electrical Engineering, National Taiwan University, Taipei 106, Taiwan.

also suppresses the undesired space-wave radiation. Moreover, the modified double-layer structure using the lossy substrate with smaller dielectric constant on the bottom can further prevent the surface-wave propagation between the upper and lower grounds of CBCTLs [27–29]. In Section 2, a distributed circuit consisting of multilayer CBCTL is proposed to model the coupled sections in filters. By applying the coupled-line and the microwave network theories, the overlapped-gap-coupled CBCTL is made equivalent to an admittance inverter for the filter design from which the analytical design formulas for the multilayer bandpass filters may be established. Section 3 illustrates the design procedure for the equal-ripple bandpass filter according to the given specifications and demonstrates the measured results. In Section 4, various types of dielectric media adopted in the single-layer or multilayer configurations are discussed. The loss mechanisms associated with dielectric, conductor, and radiation, and the far-field radiating gain patterns of space wave and surface wave are also investigated. Finally, some conclusions are drawn in Section 5.

2. DESIGN FORMULA

Fig. 1(a) shows the basic layout pattern and corresponding coordinates of the proposed multilayer coupled-line bandpass filter. Here, the input signal is fed to the conductor-backed coplanar waveguide with finite-width upper ground planes and is then coupled to the buried center conductors through the gap-coupled mechanism between the overlapped signal strips on different layers. Unlike the conventional end-coupled microstrip or CPW bandpass filters which have the open gaps on the top of the substrate, this multilayer filter structure realizing the end-coupled resonators in different dielectric layers would result in smaller radiation. The cross section and its corresponding physical dimensions with the symmetrical plane are depicted in Fig. 1(b). Usually, the input, output, and coupled CBCTLs have the same characteristic impedance of $Z_0 = 50 \Omega$. The line dimensions, such as w_1 , g_1 , w_2 , and g_2 for line sections of lengths l_1 and l_2 , can be determined by implementing the circuit on the substrates with parameters ϵ_{r1} , ϵ_{r2} , h_1 , and h_2 . To avoid the circuit discontinuities on the same layer, the CBCTLs are realized to possess the same line dimensions even on the coupled sections. Hence, the only dimensions that have to be determined for filter design are the lengths of coupled section l_{ci} and resonator l_i , $i = 1, 2$. To achieve narrower passband, the coupling should be weakened so that l_{c1} and l_{c2} are very small compared with the operating wavelength.

The design formulas are established by equating the parameters of the shorted coupled-line section with open-circuited ends to those of the π -equivalent network. The $ABCD$ matrix of the open-ended asymmetrical coupled lines with small electrical length θ_c shown in Fig. 2(a) may be approximately expressed as [30]

$$\begin{bmatrix} A & B \\ C & D \end{bmatrix} = \begin{bmatrix} \frac{R_c X + R_\pi Y}{X + Y} & \frac{X^2 + Y^2 + \left(\frac{R_c}{R_\pi} + \frac{R_\pi}{R_c}\right) XY - (X + Y)^2}{j\theta_c (X + Y)} \\ \frac{j\theta_c}{X + Y} & \frac{\frac{X}{R_c} + \frac{Y}{R_\pi}}{X + Y} \end{bmatrix} \quad (1)$$

where

$$\begin{aligned} X &= R_c \frac{Z_{c1}}{1 - \frac{R_c}{R_\pi}}, \quad Y = R_\pi \frac{Z_{\pi1}}{1 - \frac{R_\pi}{R_c}} \\ Z_{c1,\pi1} &= \frac{1}{v_{c,\pi} (c_{11} + R_{c,\pi} c_{12})} \\ v_{c,\pi} &= \left\{ \frac{a_1 + a_2}{2} \pm \frac{1}{2} \left[(a_1 - a_2)^2 + 4b_1 b_2 \right]^{1/2} \right\}^{-1/2} \\ R_{c,\pi} &= \frac{1}{2b_1} \left\{ (a_2 - a_1) \mp \left[(a_2 - a_1)^2 + 4b_1 b_2 \right]^{1/2} \right\} \end{aligned}$$

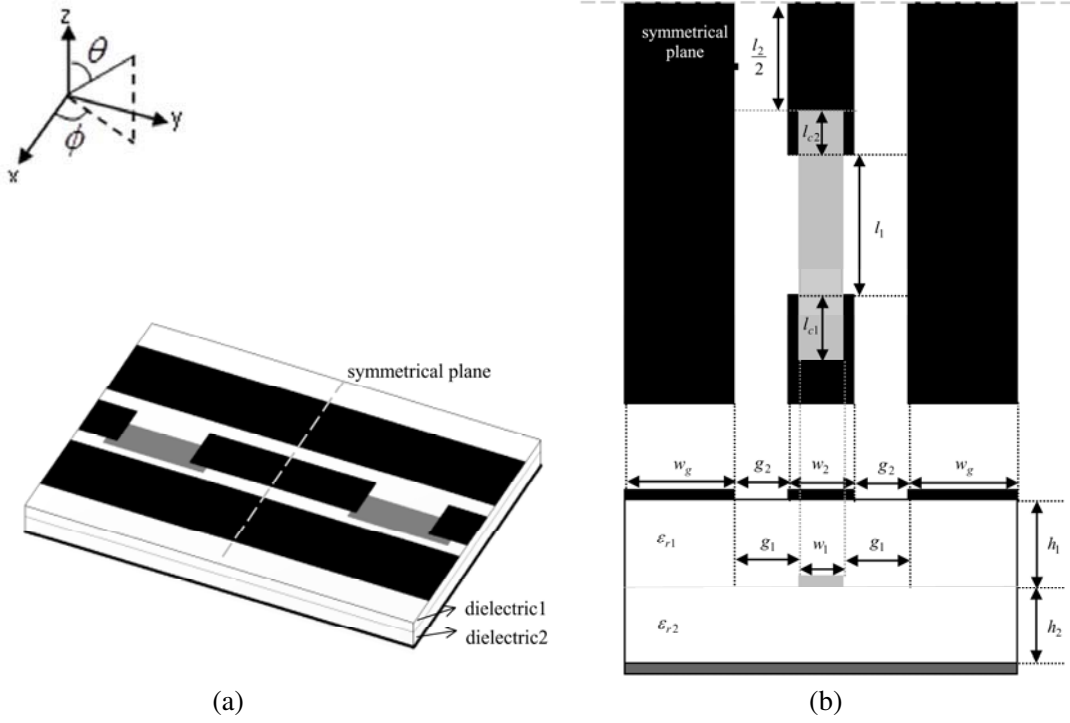


Figure 1. Multilayer gap-coupled bandpass filter. (a) Three-dimensional layout pattern. (b) Physical configuration with the corresponding cross-section.

$$a_1 = \frac{c_{11}c_{022} - c_{12}c_{012}}{v_0^2 \cdot |c_0|}$$

$$a_2 = \frac{c_{22}c_{011} - c_{12}c_{012}}{v_0^2 \cdot |c_0|}$$

$$b_1 = \frac{c_{12}c_{022} - c_{22}c_{012}}{v_0^2 \cdot |c_0|}$$

$$b_2 = \frac{c_{12}c_{011} - c_{11}c_{012}}{v_0^2 \cdot |c_0|}$$

$$|c_0| = c_{011}c_{022} - c_{012}^2$$

and v_0 is velocity of light. Here, c_{mn} and c_{0mn} , $m, n = 1, 2$, are elements of the per-unit-length capacitance matrices of the coupled CBCTLs with and without the dielectrics, respectively.

Comparing (1) with the $ABCD$ parameters of π -equivalent network shown in Fig. 2(b), the admittances can be approximately determined as

$$Y_{p1} = \frac{j\theta_c \left(\frac{X}{R_c} + \frac{Y}{R_\pi} - X - Y \right)}{\left[X^2 + Y^2 + \left(\frac{R_\pi}{R_c} + \frac{R_c}{R_\pi} \right) XY - (X + Y)^2 \right]} \quad (2)$$

$$Y_{p2} = \frac{j\theta_c (R_c X + R_\pi Y - X - Y)}{\left[X^2 + Y^2 + \left(\frac{R_\pi}{R_c} + \frac{R_c}{R_\pi} \right) XY - (X + Y)^2 \right]} \quad (3)$$

$$Y_{s2} = \frac{j\theta_c (X + Y)}{\left[X^2 + Y^2 + \left(\frac{R_\pi}{R_c} + \frac{R_c}{R_\pi} \right) XY - (X + Y)^2 \right]} \quad (4)$$

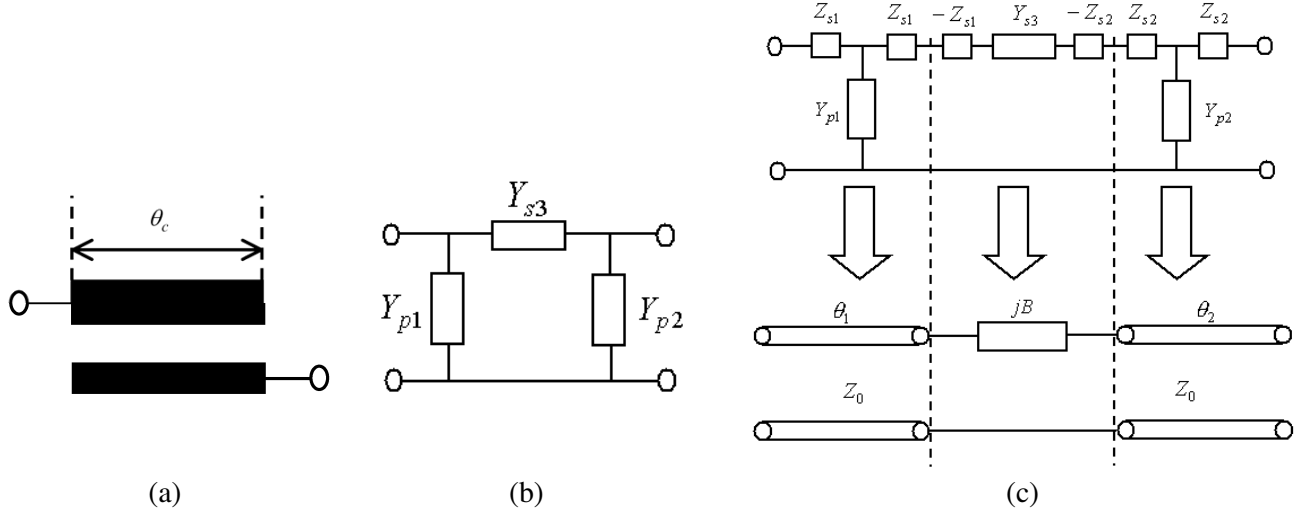


Figure 2. (a) Asymmetrical two open-ended coupled lines. (b) Corresponding π -equivalent circuit. (c) Further approximated equivalent circuit.

By adding series Z_{s1} on Y_{p1} and Z_{s2} on Y_{p2} to create the T -equivalent circuit of a cascaded transmission line, this π -connected network can be made equivalent to the one with shorted lines on either side of the series admittance jB as illustrated in Fig. 2(c). The parallel and series elements of the T -equivalent circuit of a shorted line are

$$Y_{p1} = j \frac{\sin \theta_1}{Z_0} \cong j \frac{\theta_1}{Z_0}$$

$$Y_{p2} = j \frac{\sin \theta_2}{Z_0} \cong j \frac{\theta_2}{Z_0}$$

Then Z_{s1} can be expressed as

$$Z_{s1} \cong \frac{Y_{p1} Z_0^2}{2} \quad (5)$$

$$Z_{s2} \cong \frac{Y_{p2} Z_0^2}{2} \quad (6)$$

The series admittance in Fig. 2(c) can be evaluated as

$$Y_{s3} = \frac{1}{Z_{s1} + Z_{s2} + \frac{1}{jB}} \quad (7)$$

Substituting (4), (5), and (6) into (7), the electrical length of the coupled section can be written as

$$\theta_c = \frac{\frac{1}{B} - \sqrt{\left(\frac{1}{B}\right)^2 - 2Z_0^2(\Phi + \Psi)}}{Z_0^2\Phi + Z_0^2\Psi} \cdot \Lambda \quad (8)$$

where

$$\Lambda = \left[X^2 + Y^2 + \left(\frac{R_c}{R_\pi} + \frac{R_\pi}{R_c} \right) XY - (X + Y)^2 \right] / (X + Y)$$

$$\Phi = \frac{\frac{X}{R_c} + \frac{Y}{R_\pi} - X - Y}{X + Y}$$

$$\Psi = \frac{R_c X + R_\pi Y - X - Y}{X + Y}$$

The equivalent circuit of the i -th admittance inverter J_i , $i = 1, 2$, can then be obtained by the combination of the series admittance jB_i , the shorted lines with electric lengths θ_{i1} and θ_{i2} , and the negative-length transmission lines with electrical lengths $\frac{\phi_i}{2} - \theta_{i1}$ and $\frac{\phi_i}{2} - \theta_{i2}$, as seen from Fig. 3.

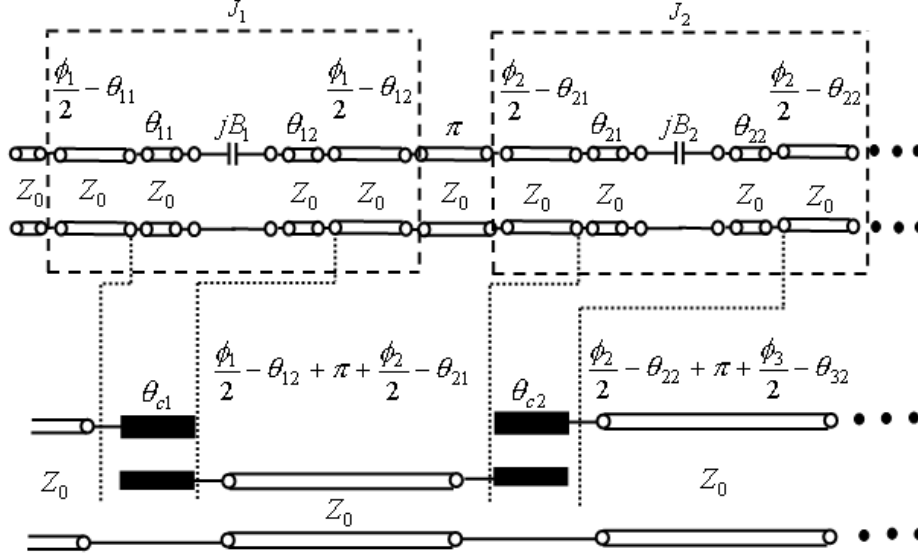


Figure 3. Transmission-line model with negative-length sections to form the admittance inverters.

Finally, the design formulas for the physical lengths of the i -th coupled section and resonator can be established [31]

$$l_{ci} = \frac{\theta_{ci}}{\sqrt{\beta_{\pi i} \beta_{ci}}} \tag{9}$$

$$l_i = \frac{1}{\beta_i} \left(\frac{\phi_i}{2} - \theta_{i,2} + \pi + \frac{\phi_{i+1}}{2} - \theta_{i+1,1} \right) \tag{10}$$

where $\phi_i = -\tan^{-1}(\frac{2Z_0 J_i}{1-(Z_0 J_i)^2})$, β_i is the phase constant of the i -th CBCTL, and β_{ci} and $\beta_{\pi i}$ are the phase constants of the c - and π -modes of the i -th coupled lines. Once the lengths of the coupled sections and the resonators are suitably modeled, the multilayer bandpass filter can be successfully designed subject to the desired specifications.

3. IMPLEMENTATION OF FILTERS

In this section, the design procedure for the multilayer filter shown in Fig. 1 is presented according to the following specifications

- characteristic impedance of the system 50Ω ,
- substrate thickness $h_1 = 0.635 \text{ mm}$ and $h_2 = 1.6 \text{ mm}$, dielectric constant $\epsilon_{r1} = 10.2$ and $\epsilon_{r2} = 4.4$, and loss tangent $\tan \delta_1 = 0.0023$ and $\tan \delta_2 = 0.016$,
- center frequency 2 GHz with a 0.5 dB equal-ripple passband characteristic,
- 3-dB bandwidth 10% ,
- attenuation at least 20 dB at 2.3 GHz .

The design procedure is summarized below:

- All the feeding and coupled CBCTLs for the specific multilayer substrates are chosen to have identical characteristic impedance 50Ω , giving the dimensions of $w_1 = 1.2 \text{ mm}$, $g_1 = 0.4 \text{ mm}$, $w_2 = 1 \text{ mm}$, $g_2 = 0.5 \text{ mm}$, and $w_g = 4 \text{ mm}$.

- The capacitance matrix of the asymmetrically coupled sections can be determined by using the coupled-line theory [32].
- The order of the filter, the elements of lowpass prototype, and the values of $Z_0 J_i$ and B_i can be determined as listed in Table 1 by using the filter synthesis technique for gap-coupled configuration [7].

Table 1. Element values for lowpass prototype and bandpass filter together with the calculated l_{cn} and $l_n \cdot l_n$ are also included.

n	g_n	$Z_0 J_n$	B_n	l_{cn}	l_n
1	1.5963	0.3137	0.00696	4.71 mm	22.07 mm
2	1.0967	0.1187	0.00241	1.46 mm	28.55 mm
3	1.5963	0.1187	0.00241	-	-
4	1.0000	0.3137	0.00696	-	-

- The lengths of coupled sections and resonators can then be determined by (9) and (10), which are $l_{c1} = 4.71$ mm, $l_{c2} = 1.46$ mm, $l_1 = 22.07$ mm, and $l_2 = 28.55$ mm.

The theoretical response shown in Fig. 4 is based on the transmission-line model (Fig. 3) by cascading the $ABCD$ matrices of the open-end coupled sections and transmission lines. To compensate the open-ended fringing effect, the section lengths should be shortened. After adjusting the geometrical dimensions for optimal response, the lengths of coupled sections and resonators are finally chosen to be $l_{c1} = 4.7$ mm, $l_{c2} = 1$ mm, $l_1 = 21.6$ mm, and $l_2 = 29.5$ mm. Fig. 4 also shows the full-wave simulated and measured S parameters of the proposed filter. The measured $|S_{21}|$ is about -1.4 dB in the passband region. Good agreement among the results of measurement, transmission-line model, and full-wave simulation validates the accuracy of the present modeling and design formulas.

4. LOSS AND RADIATION CHARACTERISTICS

To demonstrate the advantages of the proposed multilayer filters, the performances of three different bandpass filters are examined in this section. These circuit configurations are listed in Table 2, with the corresponding dimensions shown in Table 3. The finite-element electromagnetic field solver, Ansoft HFSS, is employed to investigate the loss mechanisms associated with conductor, dielectric, and radiation, as well as the far-field radiating gain patterns of space wave and surface wave of the three kinds of filters.

Table 2. Configurations for the filter types I to III (Duroid: $\epsilon_r = 10.2$, $\tan \delta = 0.0023$; FR4: $\epsilon_r = 4.4$, $\tan \delta = 0.016$).

Configuration \ Type	I	II	III
Dielectric 1	Duroid	Duroid	Duroid
Dielectric 2	Air	Air	FR4
Back Metallization	No	Yes	Yes

The time-average powers associated with the conductor, dielectric, and radiation losses are determined from the expressions

$$P_c = \frac{R_s}{2} \int_{S_c} |\overline{H}_t|^2 ds \quad (11)$$

$$P_d = \frac{1}{2} (\omega \epsilon_0 \epsilon_r \tan \delta) \int_{V_d} |\overline{E}|^2 dv \quad (12)$$

$$P_r = \frac{1}{2} \text{Re} \left(\oint_{S_o} \overline{E} \times \overline{H}^* \cdot d\overline{S} \right) \quad (13)$$

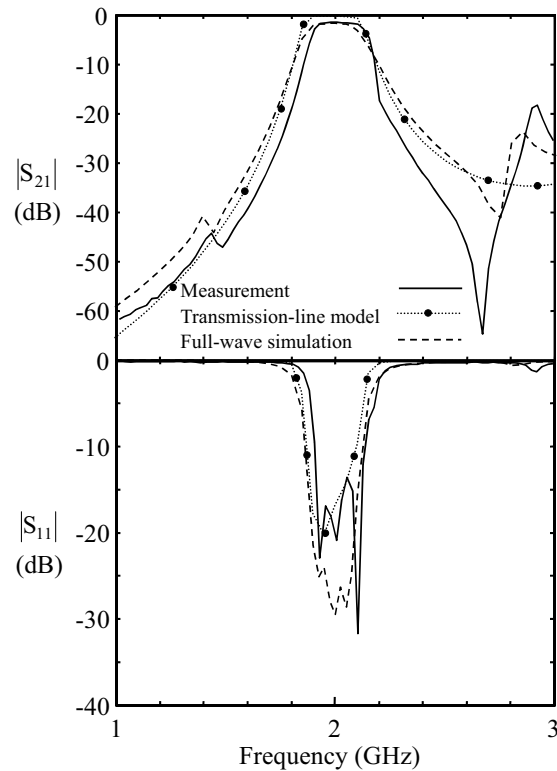


Figure 4. S -parameters of multilayer bandpass filter based on the transmission-line model, full-wave simulation, and measurement.

Table 3. Dimensions (all in millimeter) of the filter types I to III.

Dimensions \ Type	I	II	III
h_1	0.635	0.635	0.635
h_2	×	1.6	1.6
w_1	1.4	1.6	1.0
w_2	1.2	1.6	1.2
g_1	0.3	0.4	0.5
g_2	0.4	0.4	0.4
w_g	4	4	4
l_1	26.2	30.8	21.6
l_2	31.8	37.2	29.5
l_{c1}	2.8	2.2	4.7
l_{c2}	0.6	0.4	1

where $R_s = \sqrt{\frac{\omega\mu}{2\sigma}}$ is the surface resistance of the conductor and $\tan \delta$ the loss tangent of the dielectric. The surfaces S_c and S_o in (11) and (13) are the conductor surface of the filter and the absorption boundary surface enclosing the filter, respectively. Hence, the radiated power due to the space wave and surface wave can be obtained by integrating the Poynting vector through S_o . The symbol V_d in (12) represents the volume of the dielectric materials within the filter. The electric field \vec{E} , magnetic field

\bar{H} , and tangential magnetic field \bar{H}_t are available by the finite-element field solver [33].

With P_c , P_d , P_r , and the total power loss $P_{\text{total}} = P_c + P_d + P_r$ for the filter types I to III. Here, the power loss ratio represents the one normalized to the input power of the filter. The measured power loss ratio obtained by $P_L = 1 - |S_{11}|^2 - |S_{21}|^2$ is also included for comparison.

Although the type-I filter fabricated on RT Duroid 6010.2 with smaller loss tangent may decrease the dielectric loss, the radiated power loss P_r is considerably larger than P_c and P_d as shown in Fig. 6, which reveals that this significant radiation is due to the absence of back metallization. To reduce this radiation loss, the type-II filter backed by the lower ground plane is proposed. The suspended-substrate configuration is used to implement the type-II filter with the air dielectric substrate at layer 2. Due to this conductor backing, its peak radiation loss is reduced to lower than 23%, as depicted in Fig. 7. However, this air-filled configuration may excite the undesirable parallel-plate waveguide mode at 2.7 GHz and deteriorates the upper stopband response as shown in Fig. 5. The transmission zero at 2.7 GHz shown in Fig. 4 is due to the non-TEM mode excited in the inhomogeneous dielectric substrate configuration. Since the cutoff frequency of the parallel-plate mode is very low and the operating bandwidth is very wide, it is impossible to create such a wide stopband to eliminate parallel-plate mode. In this paper, the parallel-plate waveguide mode is suppressed by using the symmetrical coaxial connectors at the input and output ports and also connecting the top and bottom ground planes of the CBCTL.

To further minimize the coupling effect of the waveguide mode with the CBCTL mode, the type-III filter is proposed. This configuration, which places a thicker lossy layer (dielectric 2) on the bottom, can suppress the parasitic waveguide mode on the III dielectric 2 region without affecting the passband characteristic [34]. The suppression of waveguide mode is experimentally verified and also depicted in Fig. 5. When the half-wavelength resonators are resonating at around 2.025 GHz, the radiation and dielectric losses become larger, which results in a considerable total loss as shown in Fig. 8. The larger measured power loss is also observed except for small frequency shift. The discrepancy between P_{total} and P_L can be partly attributed to the dimensional variance and material tolerance when manufacturing the filter. In spite of this, the agreement among them is quite well, and the power loss ratio for each filter type is still reasonable.

The radiation from filter may cause serious problems in the proximity of circuits than the losses caused by conductor and dielectric. Therefore, it is interesting to further investigate the radiation characteristics of these filters, which have the same finite sized substrate and lower ground plane ($97.7 \times 30 \text{ mm}^2$). The calculated radiating gain patterns of filters on the y - z and x - y planes are illustrated in Figs. 9(a) and (b), respectively. These patterns are determined at the operating frequencies at which the power in Figs. 6–8 is maximum.

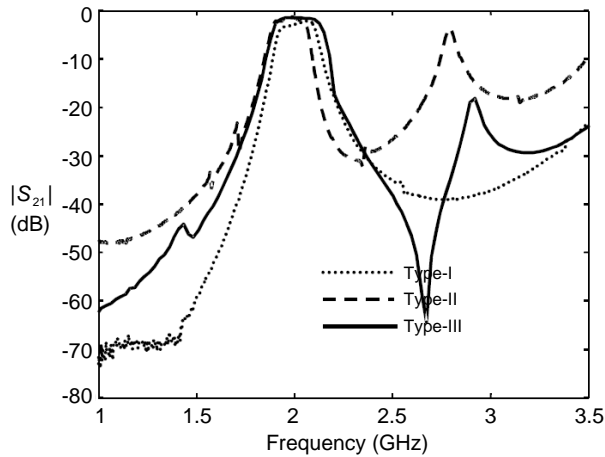


Figure 5. Measured transmission coefficients of the filter types I to III.

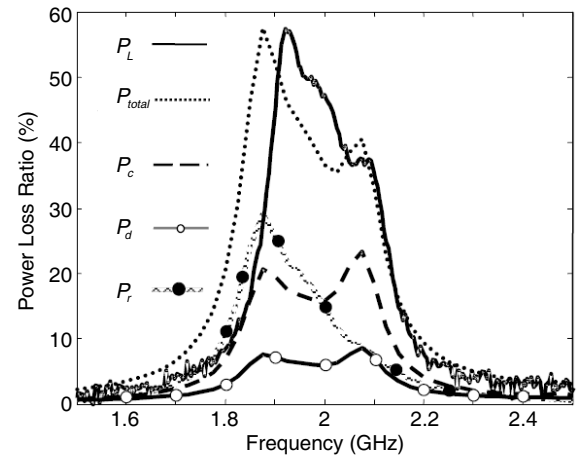


Figure 6. Calculated P_{total} , P_c , P_d , and P_r of the type-I filter. Measured P_L obtained from $1 - |S_{11}|^2 - |S_{21}|^2$ is also included.

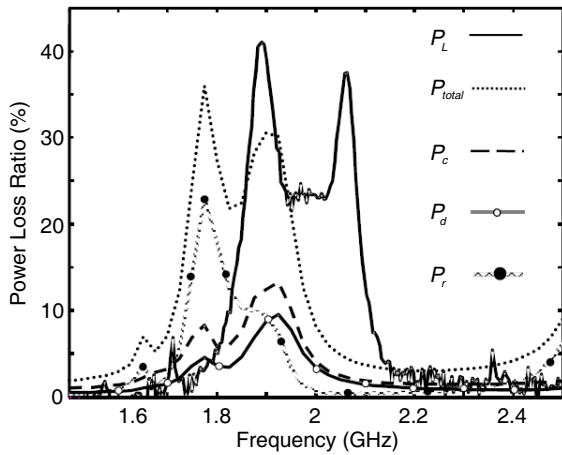


Figure 7. Calculated P_{total} , P_c , P_d , and P_r of the type-II filter. Measured P_L obtained from $1 - |S_{11}|^2 - |S_{21}|^2$ is also included.

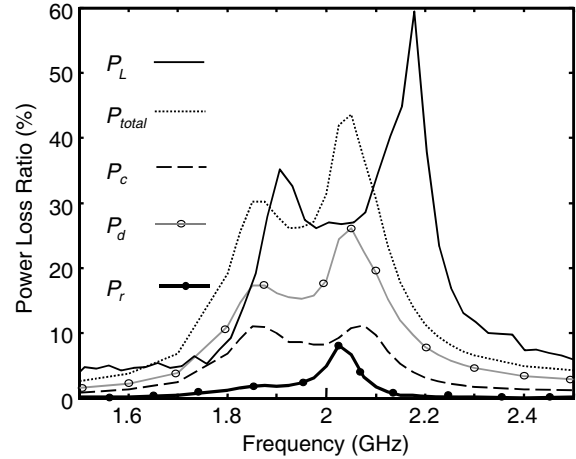


Figure 8. Calculated P_{total} , P_c , P_d , and P_r of the type-III filter. Measured P_L obtained from $1 - |S_{11}|^2 - |S_{21}|^2$ is also included.

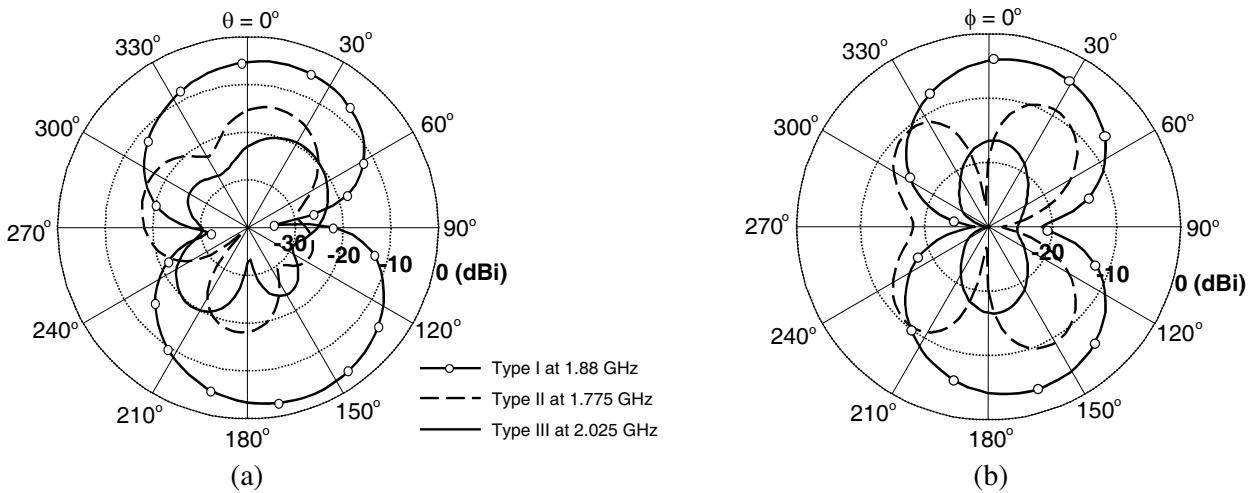


Figure 9. Far-field patterns of filter types I to III . (a) $y-z$ plane. (b) $x-y$ plane. (The corresponding coordinates are depicted in Fig. 1).

For the type-I filter, the significant radiation is mainly due to the gap discontinuities, which lead to the pattern resembling that of a short magnetic dipole as shown in Figs. 9(a) and (b). Although the type-II filter with backside conductor may reduce the radiating gain on the $y-z$ plane to lower than -15 dBi, the considerable surface wave directing at $\phi = 30^\circ$ and 150° with -8 dBi on the azimuthal plane is observed as depicted in Fig. 9(b). Compared to the results of type-I and -II filters in Fig. 9, the type-III filter has the smaller radiated power on both the $y-z$ and $x-y$ planes. Therefore, the type-III filter is attractive in suppressing the waveguide mode and improving radiation loss, thus avoiding the undesired electromagnetic interference in high-density circuits.

5. CONCLUSION

In this paper, the analytical design formulas have been developed to characterize the multilayer bandpass filter. The equivalence between the overlapped-gap-coupled CBCTL and the admittance inverter has been established. The critical dimensions of the filter, which are the lengths of coupled lines and resonators, can then be obtained by the analytical formulas that are suitable for computer-aided-design

purpose. The full-wave approach utilizing the commercial field solver and Poynting power calculation has been proposed to characterize the far-field radiating gain patterns and the power loss mechanisms caused by conductor, dielectric, and radiation. Specifically, the type-III configuration for multilayer bandpass filter has been found to be useful for minimizing the power loss and improving the stopband characteristic. Experiments have been carried out to validate the design formulas for the multilayer filter. The proposed multilayer filter with lower radiation loss and better stopband behavior is applicable to the high-performance multilayer integrated module for system-on-package applications.

REFERENCES

1. Hunter, I. C., L. Billonet, B. Jarry, and P. Guillon, "Microwave filters-applications and technology," *IEEE Trans. Microwave Theory and Tech.*, Vol. 50, 794–805, 2002.
2. Chu, P., et al., "A planar bandpass filter implemented with a hybrid structure of substrate integrated waveguide and coplanar waveguide," *IEEE Trans. Microwave Theory and Tech.*, Vol. 62, No. 2, 266–274, 2014.
3. Matthaei, G. L., "Narrow-band, fixed-tuned, and tunable bandpass filter with Zig-Zig Hairpin-COMB resonators," *IEEE Trans. Microwave Theory and Tech.*, Vol. 51, 1214–1219, 2003.
4. Cho, Y.-H. and G. M. Cho, "Two- and four-pole tunable 0.7–1.1 GHz bandpass-to-bandstop filters with bandwidth control," *IEEE Trans. Microwave Theory and Tech.*, Vol. 62, No. 3, 457–463, 2014.
5. Kuo, J.-T. and E. Shih, "Microstrip stepped impedance resonator bandpass filter with an extended optimal rejection bandwidth," *IEEE Trans. Microwave Theory and Tech.*, Vol. 51, 1554–1559, 2003.
6. Zhang, R. and L. Zhang, "Synthesis of dual-wideband bandpass filters with source-load coupling network," *IEEE Trans. Microwave Theory and Tech.*, Vol. 62, No. 3, 441–449, 2014.
7. Kuo, Y.-K., C.-H. Wang, and C. H. Chen, "Novel reduced-size coplanar-waveguide bandpass filters," *IEEE Microwave Wireless Components Lett.*, Vol. 11, 65–67, 2001.
8. Kundu, A. C. and I. Awai, "Resonant frequency and quality factors of a silver-coated $\lambda/4$ dielectric waveguide resonator," *IEEE Trans. Microwave Theory and Tech.*, Vol. 46, 11124–11131, 1998.
9. Xu, F. and K. Xu, "Understanding leaky-wave structures: A special form of guided-wave structure," *IEEE Microwave Magazine*, Vol. 14, No. 5, 87–96, 2013.
10. Boriskina, S. V. and A. I. Nosich, "Radiation and absorption losses of the whispering-gallery-mode dielectric resonators excited by a dielectric waveguide," *IEEE Trans. Microwave Theory and Tech.*, Vol. 47, 224–231, 1999.
11. Hong, J.-S. G. and M. J. Lancaster, *Microstrip Filters for RF/Microwave Applications*, John Wiley and Sons, 2001.
12. Lin, F.-L. and R.-B. Wu, "Computations for radiation and surface-wave losses in coplanar waveguide bandpass filter," *IEEE Trans. Microwave Theory and Tech.*, Vol. 47, 385–389, 1999.
13. Ikalainen, P. K. and G. L. Matthaei, "Narrow-band microstrip bandpass filters with low radiation losses for millimeter-wave applications," *IEEE Trans. Microwave Theory and Tech.*, Vol. 36, 514–521, 1988.
14. Yusuf, Y. and X. Yusuf, "Compact low-loss integration of high-Q 3-D filters with highly efficient antennas," *IEEE Trans. Microwave Theory and Tech.*, Vol. 59, No. 4, 857–865, 2011.
15. Yang, T., P. Yang, R. Chi, and W. Xu, "Folded substrate integrated waveguide based composite right/left-handed transmission line and its application to partial H -plane filters," *IEEE Trans. Microwave Theory and Tech.*, Vol. 61, No. 2, 789–799, 2013.
16. Nguyen, C., "Broadside-coupled coplanar waveguide and their end-coupled bandpass filter application," *IEEE Trans. Microwave Theory and Tech.*, Vol. 40, 2181–2189, 1992.
17. Magerko, M. A., L. Fan, and K. Chang, "Configuration considerations for multi-layered packaged conductor-backed coplanar waveguide MICs," *1994 IEEE MTT-S Int. Microwave Symp. Dig.*, 1697–1700, 1994.
18. Warns, C., W. Menzel, and H. Schumacher, "Transmission lines and passive elements for multilayer coplanar circuits on silicon," *IEEE Trans. Microwave Theory and Tech.*, Vol. 46, 616–622, 1998.

19. Sutono, A., J. Laskar, and W. R. Smith, "Design of miniature multilayer on-package integrated image-reject filters," *IEEE Trans. Microwave Theory and Tech.*, Vol. 51, 156–162, 2003.
20. Qian, S., G. Qian, J. Brand, and P. Hong, "The design of miniature multilayer bandpass filters with mixed couplings," *IEEE Trans. Microwave Theory and Tech.*, Vol. 61, No. 12, 4072–4078, 2013.
21. Davis, M. F., A. Sutono, S.-W. Yoon, S. Mandal, N. Bushyager, C.-H. Lee, K. Lim, S. Pinel, M. Maeng, A. Obatoyinbo, S. Chakraborty, J. Laskar, E. M. Tentzeris, T. Nonaka, and R. R. Tummala, "Integrated RF architectures in fully-organic SOP technology," *IEEE Trans. Adv. Packag.*, Vol. 25, 136–142, 2002.
22. Cho, C. and K. C. Gupta, "Design methodology for multilayer coupled line filter," *1997 IEEE MTT-S Int. Microwave Symp. Dig.*, 785–788, 1997.
23. Hui, J. N., W. J. Hui, and W. Q. Feng, "Balun bandpass filter based on multilayer substrate integrated waveguide power divider," *Electronics Letters*, Vol. 48, No. 10, 571, 2012.
24. Hong, J.-S. and M. J. Lancaster, "Aperture-coupled microstrip open-loop resonators and their applications to the design of novel microstrip bandpass filters," *IEEE Trans. Microwave Theory and Tech.*, Vol. 47, 1848–1855, 1999.
25. Qian, S., "Miniature quasi-lumped-element wideband bandpass filter at 0.5–2-GHz band using multilayer liquid crystal polymer technology (Technical report)," *IEEE Trans. Microwave Theory and Tech.*, Vol. 60, No. 9, 2799, 2012.
26. Mao, S.-G. and M.-Y. Chen, "Propagation characteristics of finite-width conductor-backed coplanar waveguides with periodic electromagnetic bandgap cells," *IEEE Trans. Microwave Theory and Tech.*, Vol. 50, 2624–2628, 2002.
27. Liu, Y., K. Cha, and T. Itoh, "Non-leaky coplanar (NLC) waveguides with conductor backing," *IEEE Trans. Microwave Theory and Tech.*, Vol. 43, 1067–1072, 1995.
28. Liu, Y. and T. Itoh, "Leakage phenomena in multilayer conductor-backed coplanar waveguide," *IEEE Microwave and Guided Wave Lett.*, Vol. 3, 426–427, 1993.
29. Das, N. K., "Methods of suppression or avoidance of parallel-plate power leakage from conductor-backed transmission lines," *IEEE Trans. Microwave Theory and Tech.*, Vol. 44, 169–181, 1996.
30. Tripathi, V. K., "Asymmetric coupled transmission lines in an inhomogeneous medium," *IEEE Trans. Microwave Theory and Tech.*, Vol. 23, 734–739, 1975.
31. Losch, I. E. and J. A. G. Malherbe, "Design procedure for inhomogeneous coupled line sections," *IEEE Trans. Microwave Theory and Tech.*, Vol. 36, 1186–1190, 1988.
32. Magnusson, P. C., G. C. Alexander, and V. K. Tripathi, *Transmission Lines and Wave Propagation*, 4th edition, CRC Press, 2000.
33. Shino, N. and Z. Popovic, "Radiation from ground-plane photonic bandgap microstrip waveguides," *2002 IEEE MTT-S Int. Microwave Symp. Dig.*, 1079–1082, 2002.
34. Kim, S.-J., H.-S. Yoon, and H.-Y. Lee, "Suppression of leakage resonance in coplanar MMIC packages using a Si sub-mount layer," *IEEE Trans. Microwave Theory and Tech.*, Vol. 48, 2664–2669, 2000.